LETTERS

Scalable multiparticle entanglement of trapped ions

H. Häffner[1,3], W. Hänsel[1], C. F. Roos[1,3], J. Benhelm[1,3], D. Chek-al-kar[1], M. Chwalla[1], T. Körber[1,3], U. D. Rapol[1,3], M. Riebe[1], P. O. Schmidt[1], C. Becher[1]†, O. Gühne[3], W. Dür[2,3] & R. Blatt[1,3]

The generation, manipulation and fundamental understanding of entanglement lies at the very heart of quantum mechanics. Entangled particles are non-interacting but are described by a common wavefunction; consequently, individual particles are not independent of each other and their quantum properties are inextricably interwoven[1–3]. The intriguing features of entanglement become particularly evident if the particles can be individually controlled and physically separated. However, both the experimental realization and characterization of entanglement become exceedingly difficult for systems with many particles. The main difficulty is to manipulate and detect the quantum state of individual particles as well as to control the interaction between them. So far, entanglement of four ions[4] or five photons[5] has been demonstrated experimentally. The creation of scalable multiparticle entanglement demands a non-exponential scaling of resources with particle number. Among the various kinds of entangled states, the 'W state'[6–8] plays an important role as its entanglement is maximally persistent and robust even under particle loss. Such states are central as a resource in quantum information processing[9] and multiparty quantum communication. Here we report the scalable and deterministic generation of four-, five-, six-, seven- and eight-particle entangled states of the W type with trapped ions. We obtain the maximum possible information on these states by performing full characterization via state tomography[10], using individual control and detection of the ions. A detailed analysis proves that the entanglement is genuine. The availability of such multiparticle entangled states, together with full information in the form of their density matrices, creates a test-bed for theoretical studies of multiparticle entanglement. Independently, 'Greenberger–Horne–Zeilinger' entangled states[11] with up to six ions have been created and analysed in Boulder[12].

We consider particles with the two levels $|S\rangle$ and $|D\rangle$. Then an N-particle W state

$$|W_N\rangle = (|D\cdots DDS\rangle + |D\cdots DSD\rangle + |D\cdots DSDD\rangle$$
$$+ \cdots + |SD\cdots D\rangle)/\sqrt{N} \quad (1)$$

consists of a superposition of N states where exactly one particle is in the $|S\rangle$ state while all others are in $|D\rangle$ (refs 6, 7). W states are N-particle entangled states of special interest: their entanglement is not only maximally persistent and robust under particle loss[13], but also immune against global dephasing, and rather robust against bit flip noise. Because of this robustness, W states may lead to stronger non-classicality[14] than GHZ states[11] for large numbers of particles. In addition, they may also be used for quantum communication[15–17].

The generation of such W states is performed in an ion-trap quantum processor[18]. We trap strings of up to eight $^{40}\text{Ca}^+$ ions in a linear Paul trap. Superpositions of the $S_{1/2}$ ground state and the metastable $D_{5/2}$ state of the Ca^+ ions (lifetime of the $|D\rangle$ level:

$\tau \approx 1.16$ s) represent the qubits. Each ion qubit in the linear string is individually addressed by a series of tightly focused laser pulses on the $|S\rangle \equiv S_{1/2}(m_j = -1/2) \leftrightarrow |D\rangle \equiv D_{5/2}(m_j = -1/2)$ quadrupole transition employing narrowband laser radiation near 729 nm. Doppler cooling on the fast $S \leftrightarrow P$ transition (lifetime $\sim$8 ns) and subsequent sideband cooling prepare the ion string in the ground state of the centre-of-mass vibrational mode[18]. Optical pumping initializes the ions' electronic qubit states in the $|S\rangle$ state. After preparing an entangled state with a series of laser pulses, the quantum state is read out with a CCD camera using state selective fluorescence[18].

The W states are efficiently generated by sharing one motional quantum between the ions with partial swap operations (see Table 1)[8]. For an increasing number of ions, however, the initialization of the quantum register becomes more and more difficult as technical imperfections—like incomplete optical pumping—add up for each ion. Therefore, for $N = 6,7,8$, we first prepare the state $|0, DD\cdots D\rangle$ with N π pulses on the carrier transition[18], where the 0 refers to the motional state of the centre-of-mass mode. Then, laser light resonant with the $S \leftrightarrow P$ transition projects the ion string on the measurement basis. Absence of fluorescence indicates that all ions are prepared in $|D\rangle$. Similarly, we test the motional state with a single π pulse on the blue sideband[18]. Absence of fluorescence during a subsequent detection period indicates ground state occupation. Success of both checks (total success rate $\geq$0.7) confirms that the desired initial state $|0, DD\cdots D\rangle$ is indeed prepared. We can then start with the actual entangling procedure (step (1) in Table 1) and create $|W_N\rangle$ states ($N \leq 8$) in about 500–1,000 μs.

Full information of the N-ion entangled state is obtained via quantum state reconstruction by expanding the density matrix in a basis of observables[19] and measuring the corresponding expectation values. In order to do this, we employ additional laser pulses to rotate the measurement basis prior to state detection[10]. We use 3^N different bases and repeat the experiment at least 100 times for each basis. For $N = 8$, this amounts to $\geq$656,100 experiments and a total measurement time of 10 hours. To obtain a positive semi-definite density matrix ρ, we follow the iterative procedure outlined in ref. 20 for performing a maximum-likelihood estimation of ρ. The reconstructed density matrix for $N = 8$ is displayed in Fig. 1. To retrieve the fidelity $F = \langle W_N|\rho|W_N\rangle$, we adjust the local phases such that F is maximized (see Methods). The local character of those transformations implies that the amount of entanglement present in the system is not changed. We obtain fidelities $F_4 = 0.85$, $F_5 = 0.76$, $F_6 = 0.79$, $F_7 = 0.76$ and $F_8 = 0.72$ for the 4-, 5-, 6-, 7- and 8-ion W states, respectively.

The probabilistic nature of the measurement process requires an infinite number of measurements for a perfect reconstruction of the density matrix. In order to assess the error introduced by the finite number of measurements (quantum projection noise), we have used a Monte Carlo simulation to create up to 100 comparable data sets.

[1]Institut für Experimentalphysik, [2]Institut für Theoretische Physik, Universität Innsbruck, Technikerstraße 25, A-6020 Innsbruck, Austria. [3]Institut für Quantenoptik und Quanteninformation der Österreichischen Akademie der Wissenschaften, Technikerstraße 21a, A-6020 Innsbruck, Austria. †Present address: Fachrichtung Technische Physik, Universität des Saarlandes, Postfach 151150, D-66041 Saarbrücken, Germany.

Table 1 | Creation of a $|W_N\rangle$-state ($N = \{6,7,8\}$)

Initialization		Entanglement	
	$|0, SSS\cdots S\rangle$	(1)	$\xrightarrow{R_N^+(2\arccos(1/\sqrt{N}))}$
(i1)	$\xrightarrow{R_N^C(\pi)R_{N-1}^C(\pi)\cdots R_1^C(\pi)}$		$\frac{1}{\sqrt{N}}|0, SDD\cdots D\rangle + \frac{\sqrt{N-1}}{\sqrt{N}}|1, DDD\cdots D\rangle$
	$|0, DDD\cdots D\rangle$	(2)	$\xrightarrow{R_{N-1}^+(2\arcsin(1/\sqrt{N-1}))}$
	Check state via fluorescence		$\frac{1}{\sqrt{N}}|0, SDD\cdots D\rangle + \frac{1}{\sqrt{N}}|0, DSD\cdots D\rangle + \frac{\sqrt{N-2}}{\sqrt{N}}|1, DDD\cdots D\rangle$
(i2)	$\xrightarrow{R_1^+(\pi)}$	$\vdots$	$\vdots$
	$|0, DDD\cdots D\rangle$		$\frac{1}{\sqrt{N}}|0, SDD\cdots D\rangle + \frac{1}{\sqrt{N}}|0, DSD\cdots D\rangle + \cdots + \frac{1}{\sqrt{N}}|1, DDD\cdots D\rangle$
	Check state via fluorescence	(N)	$\xrightarrow{R_1^+(2\arcsin(1/\sqrt{1}))}$
(i3)	$\xrightarrow{R_N^C(\pi)}$		$\frac{1}{\sqrt{N}}|0, SDD\cdots D\rangle + \frac{1}{\sqrt{N}}|0, DSD\cdots D\rangle + \cdots + \frac{1}{\sqrt{N}}|0, DDD\cdots S\rangle$
	$|0, SDD\cdots D\rangle$		

(i1)–(i3) are initialization steps; (1)–(N) are entanglement steps. First we initialize the ions via sideband cooling and optical pumping in the $|0, SS\cdots S\rangle$ state, where we use the notation $|n, x_N x_{N-1}\cdots x_1\rangle$. n describes the vibrational quantum number of the ion motion and x_i their electronic state. We then prepare the $|0, DDD\cdots D\rangle$ state with N π-pulses on the carrier transition applied to ions 1 to N, denoted by $R_n^C(\theta = \pi)$ (the notation is detailed in ref. 29; we do not specify the phase of the pulses because their particular value is irrelevant in this context). Then this state is checked for vanishing fluorescence with a photomultiplier tube. The same is done after trying to drive a π pulse on the blue sideband on ion 1 to ensure that the ion crystal is in the motional ground state. After this initialization, we transform the state to $|0, SDD\cdots D\rangle$ with a carrier π pulse and start the entanglement procedure in step (1). This is carried out by moving most of the population to $|1, DDD\cdots D\rangle$ with a blue sideband pulse of length $\theta_n = \arccos(1/\sqrt{n})$ leaving the desired part back in $|0, SDD\cdots D\rangle$. Finally, we use $N - 1$ blue sideband pulses ($R_n^+(\theta_n)$) of pulse length $\theta_n = \arcsin(1/\sqrt{n})$ such that at each step we split off a certain fraction of the wave packet. Note that for an ion string in the ground state, blue-sideband pulses acting on an ion in the D state have no effect. For $N = \{4,5\}$ we do not check the fluorescence, combine steps (i1) and (i3) and omit step (i2).

These data have been generated assuming ideal measurements on the reconstructed density matrix and using the measurement settings of the real experiment. For each of the artificial measurement sets a new density matrix was reconstructed via the maximum-likelihood method, and the spread of the expectation values of the observables was extracted.

For an investigation of the entanglement properties, we associate each particle k of a state ρ with a (possibly spatially separated) party A_k. We shall be interested in different aspects of entanglement between parties A_k, that is, the non-locality of the state ρ. A detailed entanglement analysis is achieved by investigating (1) the presence of genuine multipartite entanglement, (2) the distillability of multipartite entanglement and (3) entanglement in reduced states of two qubits.

First, we consider whether the production of a single copy of the state requires non-local interactions of all parties. This leads to the notion of multipartite entanglement and biseparability. A pure multipartite state $|\psi\rangle$ is called biseparable if two groups G_1 and G_2 within the parties A_k can be found such that $|\psi\rangle$ is a product state with respect to the partition

$$|\psi\rangle = |\chi\rangle_{G_1} \otimes |\eta\rangle_{G_2} \qquad (2)$$

otherwise it is multipartite entangled. A mixed state ρ is called biseparable if it can be produced by mixing pure biseparable states $|\psi_i^{bs}\rangle$—which may be biseparable with respect to different bipartitions—with some probabilities p_i, that is, the state can be written as $\rho = \sum_i p_i |\psi_i^{bs}\rangle\langle\psi_i^{bs}|$. If this is not the case, ρ is multipartite entangled. The generation of such a genuine multipartite entangled state requires interaction between all parties. In particular, a mixture of bipartite entangled states is not considered to be multipartite entangled. In order to show the presence of multipartite entanglement, we use the method of entanglement witnesses[21–23]. An entanglement witness for multipartite entanglement is an observable with a positive expectation value on all biseparable states. Thus a negative expectation value proves the presence of multipartite entanglement. A typical witness for the states $|W_N\rangle$ would be[23]:

$$\mathcal{W}_N = \frac{N-1}{N}\mathbb{1} - |W_N\rangle\langle W_N| \qquad (3)$$

This witness detects a state as entangled if the fidelity of the W state exceeds $(N-1)/N$. However, more sophisticated witnesses can be constructed, if there is more information available on the state under

investigation than only the fidelity. To do so, we add other operators to the witness in equation (3) (see Methods) which take into account that certain biseparable states can be excluded on the grounds of the measured density matrix. Table 2 lists the expectation values for these advanced witnesses. The negative expectation values prove that in our experiment four-, five-, six-, seven- and eight-qubit entanglement has been produced.

Second, we consider the question of whether one can use many copies of the state ρ to distil one pure multipartite entangled state $|\psi\rangle$ by local means; that is, whether entanglement contained in ρ is qualitatively equivalent to multiparty pure state entanglement. For this aim one determines whether there exists a number M such that the transformation

$$\underbrace{\rho \otimes \rho \otimes \cdots \otimes \rho}_{M \text{ copies}} \xrightarrow{\text{LOCC}} |\psi\rangle \qquad (4)$$

is possible. Here, $|\psi\rangle$ is a multipartite entangled pure state (for
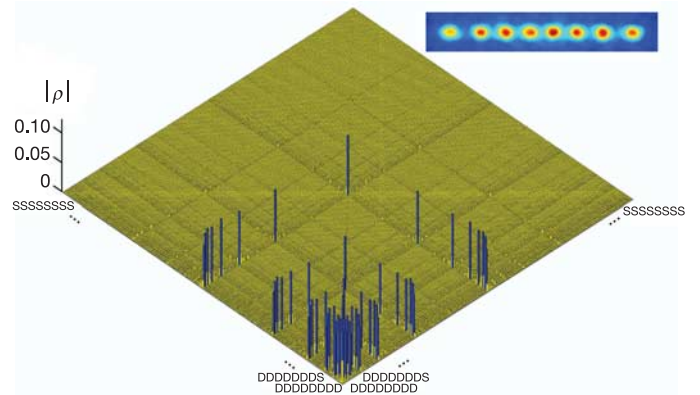
Figure 1 | Absolute values, $|\rho|$, of the reconstructed density matrix of a $|W_8\rangle$ state as obtained from quantum state tomography.
DDDDDDDD…SSSSSSSS label the entries of the density matrix ρ. Ideally, the blue coloured entries all have the same height of 0.125; the yellow coloured bars indicate noise. Numerical values of the density matrices for $4 \le N \le 8$ can be found in Supplementary Information. In the upper right corner a string of eight trapped ions is shown.

Table 2 | Entanglement properties of ρ_N

Property	$N = 3$	$N = 4$	$N = 5$	$N = 6$	$N = 7$	$N = 8$
F	0.824	0.846 (11)	0.759 (7)	0.788 (5)	0.763 (3)	0.722 (1)
$\mathrm{tr}(\tilde{\mathcal{W}}_N\rho_N)$	-0.532	-0.460 (31)	-0.202 (27)	-0.271 (31)	-0.071 (32)	-0.029 (8)
$\min(C_{kl})$	0.724	0.760 (34)	0.605 (23)	0.567 (16)	0.589 (9)	0.536 (8)
$\bar{C}$	0.776	0.794 (23)	0.683 (15)	0.677 (11)	0.668 (5)	0.633 (3)
$\min(C'_{kl})$	0.294	0.229 (21)	0.067 (12)	0.049 (4)	0.035 (4)	0.022 (3)
$\bar{C}'$	0.366	0.267 (12)	0.162 (6)	0.124 (3)	0.091 (2)	0.073 (1)

First row: fidelity after adjusting local phases (see Methods). Second row: expectation value of the witnesses $\tilde{\mathcal{W}}_N$ (for $N = 8$, we additionally used local filters). Third and fourth row: respectively minimal and average concurrence between two qubits after observing the $|D\rangle$ state on the remaining ($N - 2$) qubits. Fifth and sixth row: respectively minimal and average concurrence between two qubits after discarding the remaining ($N - 2$) qubits. For completeness, we also analysed the data published previously in ref. 8 for $N = 3$.

example, $|\psi\rangle = |W_N\rangle$) and LOCC denotes a transformation using only local operations (with respect to the parties A_k) and classical communication. If such a transformation is possible, we call the state ρ multipartite distillable[24].

Technically, multipartite distillability follows from the possibility of generating maximally entangled singlet states $|\psi^-\rangle = (|DS\rangle - |SD\rangle)/\sqrt{2}$ between any pair of parties A_k, A_l by local means[24]. The latter can readily be shown for all reconstructed density matrices. Performing measurements on all particles except k, l and restricting to outcomes $P_0 = |D\rangle\langle D|$ in all cases results in the creation of a two-qubit state ρ_{kl}. The density operator ρ_{kl} is distillable entangled if the concurrence C, a measure for two-qubit entanglement[25], is non-zero. This is the case for all k, l (see Table 2), which implies that ρ_N is multiparty distillable entangled. We remark that in practice one might use multiparticle entanglement purification protocols[26] to distil arbitrary entangled states.

Third, we investigate bipartite aspects of multiparticle entanglement[27], in particular the entanglement in the reduced states of two qubits. For W states this is of special interest, since for these states all reduced density operators of two particles are entangled, and the entanglement is in fact maximal[6,28]. We investigate the bipartite entanglement by tracing out all but particles k, l and obtain the reduced density operators ρ'_{kl}. From these density matrices, we can now calculate the concurrence $C'_{kl} = C(\rho'_{kl})$ as a measure for the entanglement. For all N, we find that all reduced density operators are entangled (see Table 2). Note that the previous results (presence of multipartite entanglement and distillability) also imply that ρ is inseparable and in fact distillable with respect to any bipartition G_1–G_2 for all N.

Last, we address the scalability of our approach. Four major sources of deviations from the ideal W states are found: addressing errors, imperfect optical pumping, non-resonant excitations and frequency stability of the qubit-manipulation laser (see Methods). All of them are purely technical and thus do not represent fundamental obstacles to increasing the number of particles. We also note that the witnesses used to detect the multipartite entanglement do not require knowledge of the full density matrix. In particular, only $1 + 2N^2$ measurement settings are sufficient to determine the witnesses' expectation value[23]. Thus the number of measurement settings does not increase exponentially with the number of particles. Also, the required blue sideband pulse area for a $|W\rangle$ state scales only with $\log N$ (see Table 1) while the time for a pulse with a given area is proportional to the square root of the ion crystal's mass, that is, to $\sqrt{N}$. Thus the overall favourable scaling behaviour of $\sqrt{N} \log N$ opens a way to study large-scale entanglement experimentally.

METHODS

Entanglement witness construction. Experimentally we do not create the W state given in equation (1), but rather a W state of the more general form

$$|\bar{W}_N\rangle = (e^{i\varphi_1}|D\cdots DDS\rangle + e^{i\varphi_2}|D\cdots DSD\rangle + \cdots + e^{i\varphi_{N-1}}|DSD\cdots D\rangle + \cdots + e^{i(\varphi_N+\pi)}|SD\cdots D\rangle)/\sqrt{N} \tag{5}$$

in which each ion has a different (local) phase φ_i. To determine the fidelity, we adjust these phases to maximize the overlap of the experimentally created W

state with $|\bar{W}_N\rangle$. These small ($\varphi_i < 15°$) phases appear because of a residual magnetic field gradient across the ion crystal and ac-Stark shifts induced by the laser pulses. Importantly, these effects are found to be constant and thus could be corrected for experimentally.

Witnesses for our experiment can be derived as follows: for N qubits we define the N states $|BS_i\rangle = |D\rangle_i \otimes |W_{N-1}\rangle$, which consist of $|D\rangle$ on the ith qubit and the state $|W_{N-1}\rangle$ on the remaining qubits. For the operator

$$\mathcal{Q} = \alpha|W_N\rangle\langle W_N| - \beta \sum_{i=1}^{N} |BS_i\rangle\langle BS_i| \tag{6}$$

we then compute the maximal expectation value for biseparable states. Since mixed biseparable states are convex combinations of pure biseparable states, it suffices to look at pure biseparable states, and thus we have to compute $\gamma = \max_{|\psi\rangle = |a\rangle \otimes |b\rangle} \langle \psi|\mathcal{Q}|\psi\rangle$ for all possible bipartitions[23]. If we investigate a partition where $|a\rangle$ is a K-qubit state, it can be seen that the optimum $|a\rangle$ is of the form $|a\rangle = a_0|DD\cdots D\rangle + b_1|DD\cdots DS\rangle + b_2|D\cdots DSD\rangle + \cdots + b_K|SDD\cdots D\rangle$. Then, from the matrix representation of $\mathcal{Q}$ one can deduce that the $a_0, b_1, \ldots, b_K$ can be chosen real and finally that $b_i = b_j$ for all i, j. A similar statement can be proven for $|b\rangle$, thus for an arbitrary number of qubits the optimization procedure can be reduced to a four-parameter maximization with two normalization constraints, which can be efficiently solved numerically. The witness is then given by

$$\tilde{\mathcal{W}}_N = \gamma \mathbb{1}_2 - \mathcal{Q} \tag{7}$$

where $\mathbb{1}_2$ denotes the identity operator on the space spanned by the elements of the computational basis which consists of $|S\rangle$ on at most two qubits. Adding the term $\gamma\mathbb{1}_2$ guarantees that $\tilde{\mathcal{W}}_N$ is positive on all biseparable states. For the entanglement detection, we used the values $\alpha = 10$ and for $\beta = 2.98$, $\gamma = 2.2598$ for three qubits, $\beta = 2.87$, $\gamma = 0.8316$ for four qubits, $\beta = 2.35$, $\gamma = 0.3760$ for five qubits, $\beta = 1.94$, $\gamma = 0.1937$ for six qubits, $\beta = 1.638$, $\gamma = 0.1139$ for seven qubits, and $\beta = 1.4125$, $\gamma = 0.0764$ for eight qubits.

For $N = 8$ we have in addition optimized the witness using local filtering operations, that is, we applied a transformation $\tilde{\mathcal{W}}_8^f = F\tilde{\mathcal{W}}_8 F^\dagger$ with $F = F_1 \otimes F_2 \otimes \cdots \otimes F_8$. Here the F_i are operators acting on each qubit separately and are thus local operations. Therefore the new witness $\tilde{\mathcal{W}}_8^f$ remains positive on all biseparable states. Finally, all witnesses have been normalized such that their expectation value for the maximally mixed state equals one and the local phases have been adjusted.

Experimental imperfections. For an investigation of the experimental imperfections, we simulate the preparation procedure by solving the Schrödinger equation with all relevant imperfections. This way, we identify four major sources of deviations from the ideal W states: addressing errors, imperfect optical pumping, non-resonant excitations, and laser frequency noise (including dephasing due to magnetic field noise). The trap frequency influences these experimental imperfections diametrically: for example, to keep the addressing error reasonably low (that is, less than 5%, where the addressing error is defined as the ratio of the Rabi frequencies between the addressed ion and the neighbouring ion(s)), we adjust the trap frequency such that the inter-ion distance in the centre of the ion string is about 5 μm. However, for large N the required reduction of the trap frequency implies that the sideband transition frequency moves closer to the carrier transition frequency. Thus the strong laser pulses driving the weak sideband transition cause more off-resonant excitations on the carrier transition, which in turn spoil the obtainable fidelity. Therefore we reduce the laser power for driving the sideband, which then results in longer preparation times and leads to an enhanced susceptibility to laser frequency noise. A compromise for the different ion numbers N is the following set of parameters: ($N = 4$: $\nu = 1.123$ MHz, $T_{2\pi} = 220$ μs), ($N = 5$: $\nu = 1.055$ MHz, $T_{2\pi} = 300$ μs), ($N = 6$: $\nu = 0.905$ MHz, $T_{2\pi} = 350$ μs), ($N = 7, 8$: $\nu = 0.813$ MHz, $T_{2\pi} = 380$ μs). Here ν is the trap frequency (centre of mass) and $T_{2\pi}$ is the time for a 2π pulse on the blue sideband. The fidelity reduction of $|W_6\rangle$ for the different imperfections are as follows: 0.1 (addressing

error), 0.07 (off-resonant excitations), 0.04 (laser frequency noise (200 Hz r.m.s.)). Another possible error source is imperfect ground state cooling. Intensity noise of the 729-nm laser ($\Delta I_{max}/I \approx 0.03$) does not contribute significantly. Finally, we experimentally observed non-ideal optical pumping, which can result in a reduction of 0.02 of the fidelity per ion. In principle, this imperfection can be eleminated by single ion detection and subsequent π pulses on the carrier transition. Currently, for $N \geq 6$, we reduce the errors due to optical pumping and a part of the addressing errors by checking the initialization procedure with a detection sequence (see Table 1).

1. Schrödinger, E. Die gegenwärtige Situation in der Quantenmechanik. *Naturwissenschaften* **23**, 807–812 (1935).
2. Schrödinger, E. Die gegenwärtige Situation in der Quantenmechanik. *Naturwissenschaften* **23**, 823–828 (1935).
3. Schrödinger, E. Die gegenwärtige Situation in der Quantenmechanik. *Naturwissenschaften* **23**, 844–849 (1935).
4. Sackett, C. A. *et al.* Experimental entanglement of four particles. *Nature* **404**, 256–259 (2000).
5. Zhao, Z. *et al.* Experimental demonstration of five-photon entanglement and open-destination teleportation. *Nature* **430**, 54–58 (2004).
6. Dür, W., Vidal, G. & Cirac, J. I. Three qubits can be entangled in two inequivalent ways. *Phys. Rev. A* **62**, 062314 (2000).
7. Zeilinger, A., Horne, M. A. & Greenberger, D. M. Higher-order quantum entanglement. *NASA Conf. Publ.* **3135**, 73–81 (1992).
8. Roos, C. F. *et al.* Control and measurement of three−qubit entangled states. *Science* **304**, 1478–1480 (2004).
9. Bennett, C. H. & DiVincenzo, D. P. Quantum information and computation. *Nature* **404**, 247–255 (2000).
10. Roos, C. F. *et al.* Bell states of atoms with ultralong lifetimes and their tomographic state analysis. *Phys. Rev. Lett.* **92**, 220402 (2004).
11. Greenberger, D. M., Horne, M. & Zeilinger, A. in *Bell's Theorem, Quantum Theory, and Conceptions of the Universe* (ed. Kafatos, M.) 69–72 (Kluwer Academic, Dordrecht, 1989).
12. Leibfried, D. *et al.* Creation of a six-atom 'Schrödinger cat' state. *Nature* doi:10.1038/nature 04251 (this issue).
13. Briegel, H. J. & Raussendorf, R. Persistent entanglement in arrays of interacting particles. *Phys. Rev. Lett.* **86**, 000910 (2001).
14. Sen(De), A. *et al.* Multiqubit W states lead to stronger nonclassicality than Greenberger−Horne−Zeilinger states. *Phys. Rev. A* **68**, 062306 (2003).
15. Joo, J., Park, Y.-J., Lee, J., Jang, J. & Kim, I. Quantum secure communication via a W state. *J. Korean Phys. Soc.* **46**, 763–768 (2005).
16. Joo, J., Lee, J., Jang, J. & Park, Y.-J. Quantum secure communication with W States. Preprint at ⟨http://arxiv.org/quant-ph/0204003⟩ (2002).
17. Buhrman, H., van Dam, W., Høyer, P. & Tapp, A. Multiparty quantum communication complexity. *Phys. Rev. A* **60**, 2737–2741 (1999).
18. Schmidt-Kaler, F. *et al.* How to realize a universal quantum gate with trapped ions. *Appl. Phys. B* **77**, 789–796 (2003).
19. Fano, U. Description of states in quantum mechanics by density matrix and operator techniques. *Rev. Mod. Phys.* **29**, 74–93 (1957).
20. Hradil, Z., Reháček, J., Fiurášek, J. & Ježek, M. Maximum-likelihood methods in quantum mechanics. *Lect. Notes Phys.* **649**, 59–112 (2004).
21. Horodecki, M., Horodecki, P. & Horodecki, R. Separability of mixed states: Necessary and sufficient conditions. *Phys. Lett. A* **223**, 1–8 (1996).
22. Terhal, B. M. Bell inequalities and the separability criterion. *Phys. Lett. A* **271**, 319–326 (2000).
23. Bourennane, M. *et al.* Experimental detection of multipartite entanglement using witness operators. *Phys. Rev. Lett.* **92**, 087902 (2004).
24. Dür, W. & Cirac, J. I. Classification of multiqubit mixed states: Separability and distillability properties. *Phys. Rev. A* **61**, 042314 (2000).
25. Wootters, W. K. Entanglement of formation of an arbitrary state of two qubits. *Phys. Rev. Lett.* **80**, 2245–2248 (1998).
26. Miyake, A. & Briegel, H.-J. Distillation of multipartite entanglement by complementary stabilizer measurements. Preprint at ⟨http://arxiv.org/quant-ph/0506092⟩ (2005).
27. Dür, W. & Cirac, J. I. Multiparticle entanglement and its experimental detection. *J. Phys. A* **34**, 6837–6850 (2001).
28. Koashi, M., Bužek, V. & Imoto, N. Entangled webs: Tight bound for symmetric sharing of entanglement. *Phys. Rev. A* **62**, 050302 (2000).
29. Gulde, S. *et al.* Implementing the Deutsch-Jozsa algorithm on an ion-trap quantum computer. *Nature* **421**, 48–50 (2003).